14th International Symposium on Turbulence and Shear Flow Phenomena (TSFP14)
Heidelberg, Germany, July 28–31, 2026

LARGE EDDY SIMULATION OF BURGULENCE CONCEPTUALIZED AS A SYNTHESIS OF FILTERING, MODELING AND DISCRETIZATION

Roel Verstappen
Bernoulli Institute for Mathematics, Computer Science and Artificial Intelligence
University of Groningen
Nijenborgh 9, 9747 AG Groningen, The Netherlands
r.w.c.p.verstappen@rug.nl

ABSTRACT

Large Eddy Simulation (LES) of burgulence is conceptualized as a synthesis of filtering, modeling and discretization. Small-scale motions are removed by applying conservation laws over control volumes of user-defined size, establishing the computational grid. Two spatial filters emerge: one from grid-cell averaging and another from interpolating fluxes at cell faces. The interpolation filter defines the large eddies, while a model captures the net effect of smaller scales. This model bridges physical and numerical interpretations which converge when filtering, modeling, and discretization are treated coherently, i.e., constitute a unified methodological approach. The two filters partition kinetic energy into three: the subgrid part, the large-eddy part, and the supergrid part filtered-out by cell-to-face interpolation. The latter scales are subordinate to the large eddies. The model ensures that large eddies do not generate smaller scales, with consistency enhanced via extrapolation. The approach is validated on 1D decaying Burgers' turbulence.

FILTERING, MODELING, DISCRETIZATION

Since its introduction in 1963, Large eddy simulation (LES) has advanced significantly and has developed into a valuable tool to study turbulent flow. LES resolves only motions larger than a prescribed length scale and models the combined (dissipative) effect of the unresolved motions. The model for unresolved small-scale turbulence and the numerical discretization of the governing equations are often treated as modular components, each replaceable by alternatives with equivalent functionality. However, this modularity overlooks the complex nonlinear interactions between modeling and discretization errors, which remain poorly understood yet critically influence overall simulation accuracy, see Geurts (2009), e.g. In practice, the boundaries between filtering, modeling and discretization become blurred, as numerical schemes influence both the effective filter and the modeled dissipation. This work therefore treats the core elements of LES as a unified whole; it seeks to advance LES through the integration of filtering, modeling and discretization. The integrated approach is developed and demonstrated for LES of Burgers' turbulence in one spatial dimension, serving as an initial step toward future extensions to three-dimensional turbulent flows.

PHYSICAL AND NUMERICAL MODEL

Pope (2004) posed the question *Is LES a physical model, a numerical procedure or a combination of both?* The answer remains debated. One view holds that the small-scale model is physical and should be treated as part of the governing PDEs, which are then discretized. The opposing view argues that no explicit physical model is needed because the numerical method can supply the required dissipation. A further complication is the ordering of filtering and discretization: filtering is typically applied first and discretization last, but the reverse order is also possible, see Agdestein & Sanderse (2025). In this paper, LES of Burgers' turbulence is formulated in a way that allows it to be viewed either as a physical model or as a numerical one. To illustrate both perpectives, we introduce the box filter

$$\overline{\phi}(x,t) = \frac{1}{\delta}\int_{x-\frac{\delta}{2}}^{x+\frac{\delta}{2}} \phi(\xi,t)\,d\xi, \tag{1}$$

where the filter length δ is to be chosen by the user. The time-rate of change of $\overline{\phi}$ is governed by a conservation law. Assuming, for simplicity, that the density ϕ is advected only by a velocity u, we obtain

$$\delta\,\partial_t\overline{\phi}(x,t) = (u\phi)(x-\tfrac{\delta}{2}) - (u\phi)(x+\tfrac{\delta}{2}). \tag{2}$$

The right-hand side depends on unfiltered quantities. To approximate it using filtered quantities, we introduce a model $\tau(\overline{u},\overline{\phi}) \approx u\phi - \overline{u}\overline{\phi}$. With the help of this model, we arrive at

$$\delta\,\partial_t\overline{\phi}(x,t) = (\overline{u}\overline{\phi}+\tau)(x-\tfrac{\delta}{2}) - (\overline{u}\overline{\phi}+\tau)(x+\tfrac{\delta}{2}). \tag{3}$$

So far we viewed τ as a *physical* model that (approximately) describes the nonlinear effect of all scales of motion that are filtered out by taking $\overline{\phi}$ instead of ϕ and $\overline{u}$ instead of u. That's one way to look at it. Alternatively, we can view τ as a *numerical* model. To develop that perspective, we apply a finite volume method (FVM) to discretize the conservation law. For simplicity we consider a uniform grid with spacing h. The gridpoints are denoted by $x_i = ih$ and the i-th finite 'volume' is $[x_{i-1},x_i]$ with $i = 1,\ldots,N$. The finite volume method represents the density by

$$\widetilde{\phi}_{i-1/2}(t) = \frac{1}{h}\int_{x_{i-1}}^{x_i} \phi(x,t)\,dx \tag{4}$$

In the context of LES Eq. (4) is seen as a box filter with filter length h. We denote it by a tilde to stress that the filter length

is h, not δ. The conservation law yields

$$h\partial_t \widetilde{\phi}_{i-1/2} = (u\phi)_{i-1} - (u\phi)_i. \tag{5}$$

where $(u\phi)_i$ denotes the convective flux at x_i, that is at the right-hand side of the finite volume. Likewise $(u\phi)_{i-1}$ is the flux at the left-hand side $x = x_{i-1}$. Note that $x_{i-1/2}$ lies exactly midway between the gridpoints x_{i-1} and x_i because the grid is uniform. The core of the discretization problem is to express the density ϕ_i in terms of the filtered densities $\widetilde{\phi}_{i-1/2}$ and $\widetilde{\phi}_{i+1/2}$. For that we use the interpolation

$$\phi_i \approx \tfrac{1}{2}(\widetilde{\phi}_{i-1/2} + \widetilde{\phi}_{i+1/2}) \tag{6}$$

Taking $\delta = 2h$ yields the key relation

$$\overline{\phi}(x_i) = \overline{\phi}_i = \tfrac{1}{2}(\widetilde{\phi}_{i-1/2} + \widetilde{\phi}_{i+1/2}). \tag{7}$$

The conservation law (5) can thus be written as

$$h\,\partial_t \widetilde{\phi}_{i-1/2} = \overline{u}_{i-1}\overline{\phi}_{i-1} + \tau_{i-1} - \overline{u}_i\overline{\phi}_i - \tau_i, \tag{8}$$

where the difference $\tau_{i-1} - \tau_i$ is now the truncation error of the finite volume method: leaving out the τ's in Eq. (8) yields the usual finite volume approximation. Eq. (8) contains two filters, the grid filter (4) with length h and the box filter (1) with length $\delta = 2h$. These filters are related by Eq. (7). To obtain a conservation law containing a single filter, we consider the two neighboring 'volumes' given by $[x_{i-1}, x_i]$ and $[x_i, x_{i+1}]$. The two corresponding equations (Eq. (8) for $\widetilde{\phi}_{i-1/2}$ as well as for $\widetilde{\phi}_{i+1/2}$) can be added together using Eq. (7). This results into the conservation law

$$\delta\,\partial_t \overline{\phi}_i = \overline{u}_{i-1}\overline{\phi}_{i-1} + \tau_{i-1} - \overline{u}_{i+1}\overline{\phi}_{i+1} - \tau_{i+1}, \tag{9}$$

which uses *overlapping volumes*, see Fig. 1.
In conclusion, if the model τ on the right-hand side of Eq. (3) is interpreted as representing subfilter-scale physics, then the influence of the filtered-out scales on the dynamics of the filtered scales must be modeled physically. This model is defined for all positions x. When evaluated specifically at grid points x_i (i.e., the faces of finite volumes), the same τ represents the truncation error of the finite volume discretization (9). In this context, the unresolved scales from the interpolation rule (6) are to be considered. These perspectives highlight the parallel between physical and numerical modeling. Equation (9) is structurally identical to Eq. (3), with the distinction that (9) applies only at grid points x_i for a filter length equal to twice the grid spacing, whereas (3) holds for any x.

VISCOUS FLUX

So far no attention has been paid to viscous dissipation, because it requires the spatial derivative of ϕ. As usual, the viscous fluxes are modeled by adding $\nu\partial_x\phi(x_i,t) - \nu\partial_x\phi(x_{i-1},t)$ to the conservation law (5), where ν is the viscosity of the fluid. Our filters commutes with differentiation:

$$\partial_x\widetilde{\phi} = \frac{\phi(x+\frac{h}{2},t) - \phi(x-\frac{h}{2},t)}{h} = \widetilde{\partial_x\phi}. \tag{10}$$

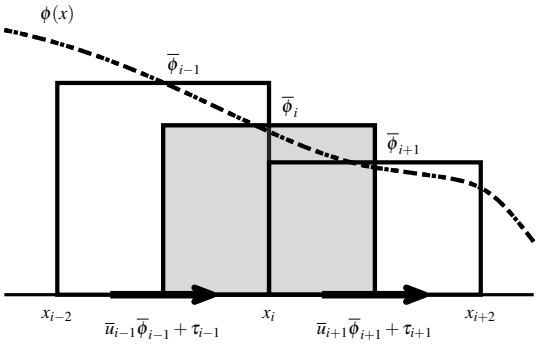

Figure 1. Illustration of the finite volume model (9). The dashed curve shows the density ϕ. The box-filtered densities are depicted as rectangles with width δ and height $\overline{\phi}_{i-1}$, $\overline{\phi}_i$ and $\overline{\phi}_{i+1}$. The arrows indicate the convective fluxes through the faces $x = x_{i-1}$ and $x = x_{i+1}$ of the control volume centered at the gridpoint x_i. These fluxes are evaluated without interpolation because the volumes partially overlap.

Hence, the derivative of ϕ can be broken down into a difference quotient of the filtered density and an unclosed term that can be included in τ:

$$\begin{aligned}\partial_x\phi &= \partial_x\widetilde{\overline{\phi}} + \partial_x(\phi - \widetilde{\overline{\phi}}) \\ &\overset{(10)}{=} \frac{\widetilde{\phi}(x+\frac{h}{2}) - \widetilde{\phi}(x-\frac{h}{2})}{h} + \partial_x(\phi - \widetilde{\overline{\phi}}).\end{aligned}$$

The quotient in the right-hand side can be regarded as a discretization of the derivative. The error in this approximation is given by $\partial_x(\phi - \overline{\overline{\phi}})$, i.e., the error of the spatial discretization is an unclosed term, and, once again, we cannot distinguish a discretization error from an unclosed term. So, also for diffusion, subfilter modeling and spatial discretization are intrinsically linked. The introduction of viscous flux into the conservation law (5) leads to a modified equation that incorporates both convective and diffusive fluxes:

$$h\,\mathrm{d}_t\widetilde{u}_{i-1/2} + \Phi_i - \Phi_{i-1} = -\tau_i + \tau_{i-1}, \tag{11}$$

where

$$\Phi_i = \overline{u}_i\overline{\phi}_i - \nu\,\frac{\widetilde{\phi}_{i+1/2} - \widetilde{\phi}_{i-1/2}}{h}, \tag{12}$$

denotes the filtered flux and

$$\tau = u\phi - \overline{u}\overline{\phi} + \nu\partial_x(\widetilde{\overline{\phi}} - \phi), \tag{13}$$

is the sub-filter flux (either LES model or FVM truncation error). This discrete LES system highlights the two filters: the average over the finite volume defines the first filter, $\widetilde{\phi}_{i-1/2}$, the cell-to-face interpolation (7) introduces the second filter $\overline{\phi}_i$. Finally, it may be remarked that this system of equations is exact, an error is introduced when τ is replaced by a model depending on filtered quantities only. It can already be noted here that τ may very well depend on $\widetilde{\phi}$ and $\widetilde{u}$, i.e., τ does not have to be limited to functions of $\overline{\phi}$ and $\overline{u}$, as has been the case until now.

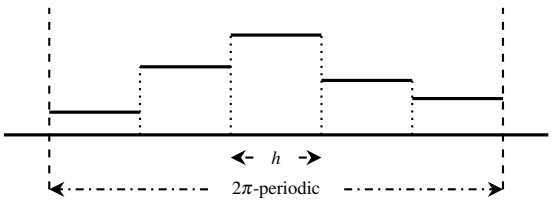

Figure 2. A characteristic function in the finite volume function space $\widetilde{\mathscr{F}_N}(0,2\pi)$.

GRID FILTER

The discrete grid filter (4) is only defined at the centers $x_{i-1/2}$ of the grid cells. We extend it to a symmetric filter that is defined for all x by means of the piecewise-constant function

$$\widetilde{\phi}_h(x,t) = \frac{1}{h}\int_{x_{i-1}}^{x_i} \phi(x,t)\,dx \overset{(4)}{=} \widetilde{\phi}_{i-1/2}(t) \qquad (14)$$

for $x_{i-1} \le x < x_i$. Filtering twice yields the same result as filtering once, indicating that the grid filter (14) removes information. When filtering $\phi = \widetilde{\phi}_h + \phi'_h$ (with ϕ'_h as the residue of the grid filter), we get $\widetilde{\phi'}_h = 0$, i.e., unresolvable scales vanish after filtering. This leads to the orthogonality

$$(\widetilde{\psi}_h, \phi'_h) = (\psi_h, \widetilde{\phi'_h}) = 0, \qquad (15)$$

for any ψ and ϕ. Hence, the function space splits orthogonally into two subspaces, a resolved space and an unresolved space. The resolved space is N-dimensional and consists of $\widetilde{\phi}_{i-1/2}(t)$ with $i = 1,...,N$, with time as a continuous variable.

CUTOFF OF SUBGRID SCALES

Eq. (15) divides the energy into a supergrid part and a subgrid part:

$$\|\phi\|_2^2 = \|\widetilde{\phi}_h\|_2^2 + \|\phi'_h\|_2^2. \qquad (16)$$

This section is about the subgrid scales of motion; the next ones deal with the supergrid scales. The (semi-)discrete densities $\widetilde{\phi}_{i-1/2}(t)$ are expanded to piecewise-constant functions $\widetilde{\phi}_h(x,t)$ as in (14) to discuss the subgrid scales of motion. The finite-volume function space $\widetilde{\mathscr{F}_N}(0,2\pi)$ is defined as the collection of functions $\widetilde{\phi}_h(x,t)$ that are 2π-periodic in x and take $[0,2\pi)\times\mathbb{R}_+$ into $\mathbb{R}$ such that $\widetilde{\phi}_h(x,t) = \widetilde{\phi}_{i-1/2}(t)$ on every interval $x_{i-1} \le x < x_i$, where $\widetilde{\phi}_{i-1/2} : \mathbb{R}_+ \mapsto \mathbb{R}$, $x_i = ih$, $h = 2\pi/N$, $i = 1,2,...,N$ and $t \ge 0$. Fig. 2 depicts a characteristic function in this space (at a time t - the dependence on t is not made explicit in the following to simplify the notation). As usual, the addition and multiplication of functions is defined pointwise. For every function $\widetilde{\phi}_h$ and $\widetilde{u}_h$ in $\widetilde{\mathscr{F}_N}(0,2\pi)$, $\widetilde{\phi}_h + \widetilde{u}_h$ also lies in $\widetilde{\mathscr{F}_N}(0,2\pi)$, as does the product $\widetilde{u}_h\widetilde{\phi}_h$!! Furthermore, if $\widetilde{\phi}_h(x) \in \widetilde{\mathscr{F}_N}(0,2\pi)$ then $\widetilde{\phi}_h(x\pm h) \in \widetilde{\mathscr{F}_N}(0,2\pi)$. Consequently,

$$\overline{\phi}_\delta(x) = \tfrac{1}{2}\left(\widetilde{\phi}_h(x+h) + \widetilde{\phi}_h(x)\right)$$

lies in $\widetilde{\mathscr{F}_N}(0,2\pi)$, for any $\widetilde{\phi}_h \in \widetilde{\mathscr{F}_N}(0,2\pi)$. Note: $\overline{\phi}_\delta(x) = \frac{1}{2}(\widetilde{\phi}_{i+1/2} + \widetilde{\phi}_{i-1/2})$ for all $x \in [x_{i-1}, x_i)$. The left-hand side is here taken at x and not at $x + h/2$ because the x coordinate cannot be translated over $h/2$ in $\widetilde{\mathscr{F}_N}(0,2\pi)$. From the above properties, it follows that the flux

$$\Phi_h(x) = \overline{u}_\delta(x)\,\overline{\phi}_\delta(x) - \nu\,\frac{\widetilde{\phi}_h(x+h) - \widetilde{\phi}_h(x)}{h}$$

lies in the finite volume function space $\widetilde{\mathscr{F}_N}(0,2\pi)$ for any $\widetilde{u}_h$ and $\widetilde{\phi}_h$ in $\widetilde{\mathscr{F}_N}(0,2\pi)$, and the same applies to the flux difference $\Phi_h(x) - \Phi_h(x-h)$. Hence, the dynamical system

$$h\,\partial_t\widetilde{\phi}_h(x) = (\Phi_h + \tau_h)(x-h) - (\Phi_h + \tau_h)(x) \qquad (17)$$

is *closed in the finite volume function space* $\widetilde{\mathscr{F}_N}(0,2\pi)$ *for any model* $\tau_h \in \widetilde{\mathscr{F}_N}(0,2\pi)$. The above-defined flux $\Phi_h(x)$ is piecewise constant, i.e., $\Phi_h(x) = \Phi_i(t)$ for $x_{i-1} \le x < x_i$, where Φ_i is given by Eq. (12). Therefore, Eq. (17) is identical to the finite volume discretization (11)-(13) for all $x \in [x_{i-1}, x_i)$ with $i = 1,2,..,N$. So, the finite-volume approximation is distinctly different from a projection on the first N Fourier-modes, for example. Such a projection results into an unclosed system as the nonlinear convective term generates Fourier modes with wave numbers larger than N. The finite volume approximation, on the other hand, is closed - the solution to Eq. (17) does not run out of the N-dimensional space $\widetilde{\mathscr{F}_N}(0,2\pi)$. This conclusion can also be expressed using the residue of the grid filter (14). From Eq. (17) it follows that $\partial_t\widetilde{\phi}_h \in \widetilde{\mathscr{F}_N}(0,2\pi)$. Therefore, the orthogonality (15) yields

$$(\partial_t\widetilde{\phi}_h, \phi'_h) = 0, \qquad (18)$$

again for any model $\tau_h \in \widetilde{\mathscr{F}_N}(0,2\pi)$. So, *the finite volume discretization (17) has a built-in mechanism that counteracts the production of subgrid scales of motion*. The unresolved, subgrid scales of motion are beyond our observation range. Eq. (18) states that they are not produced in the finite volume approach (11)-(13); hence the dissipation of energy is given by

$$\mathrm{d}_t\|\phi\|_2^2 \overset{(16)}{=} \mathrm{d}_t\|\widetilde{\phi}_h\|_2^2 + \mathrm{d}_t\|\phi'_h\|_2^2 \overset{(18)}{=} \mathrm{d}_t\|\widetilde{\phi}_h\|_2^2 \qquad (19)$$

and we can therefore focus on the supergrid scales.

DECOMPOSITION OF SUPERGRID SCALES

In this section, the supergrid density $\widetilde{\phi}$ is split into a large-eddy component $\overline{\phi}$ and a residual $\phi^\star$:

$$\widetilde{\phi}_{i-1/2} = \underbrace{\tfrac{1}{2}(\widetilde{\phi}_{i+1/2} + \widetilde{\phi}_{i-1/2})}_{\overline{\phi}_i} + \underbrace{\tfrac{1}{2}(\widetilde{\phi}_{i-1/2} - \widetilde{\phi}_{i+1/2})}_{\phi_i^\star} \qquad (20)$$

The boundary conditions must be taken into account in this splitting. Under periodic boundary conditions, i.e., $\widetilde{\phi}_{N+1/2} = \widetilde{\phi}_{1/2}$, we have

$$\sum_{i=1}^{N}(\widetilde{\phi}_{i-1/2})^2 = \sum_{i=1}^{N}(\overline{\phi}_i)^2 + \sum_{i=1}^{N}(\phi_i^\star)^2. \qquad (21)$$

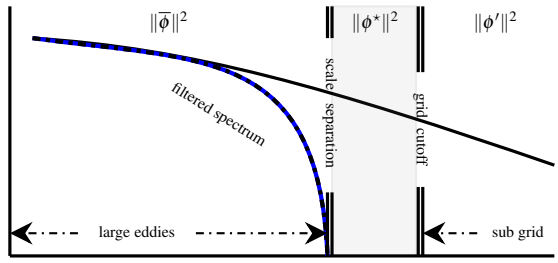

Figure 3. Sketch of the energy spectra of the full solution and that of the large eddies. The entire spectrum divides into three parts. The subgrid part $\|\phi'\|^2$ is cuttoff by the grid. The model aims to separate the supergrid energy $\|\phi^\star\|^2$ from the energy $\|\overline{\phi}\|^2$ of the large eddies.

This can be described more compactly by $||\widetilde{\phi}||^2 = ||\overline{\phi}||^2 + ||\phi^\star||^2$, where $\widetilde{\phi}$, $\overline{\phi}$ and $\phi^\star$ are vectors in $\mathbb{R}^N$ with components $\widetilde{\phi}_{i-1/2}$, $\overline{\phi}_i$ and $\phi_i^\star$ ($i = 1,..,N$), respectively. Note that the components of the vector $\widetilde{\phi}$ are defined at the cell centers, whereas the components of $\overline{\phi}$ and $\phi^\star$ are defined at the faces. Importantly, the vectors $\overline{\phi}$ and $\phi^\star$ are perpendicular,

$$\overline{\phi} \cdot \phi^\star = 0. \tag{22}$$

Moreover, $\|\phi^\star\| > 0$ implies that $\|\widetilde{\phi}\| > \|\overline{\phi}\|$. Here, $\widetilde{\phi}$ represents the density at the centers of the grid cells and $\overline{\phi}$ is the (interpolated) density at the faces. Thus $\|\phi^\star\| \neq 0$ can also be interpreted as: the length of the density vector at the cell centers is not equal to the length of the density vector at the cell faces. The norm $\|\widetilde{\phi}_h\|_2$ of $\widetilde{\phi}_h$ in Eq. (16) is defined on the function space $\widetilde{\mathscr{F}_N}(0,2\pi)$. Because $\widetilde{\phi}_h$ is piecewise constant, we have $\|\widetilde{\phi}_h\|_2^2 = h\|\widetilde{\phi}\|^2$, where $\|\ \|$ denotes the Euclidean norm on the vector space $\mathbb{R}^N$. By combining Eqs. (16)+(21) we see that the two filters (1) and (14) split the energy into three pieces

$$\|\phi\|_2^2 = h\|\overline{\phi}\|^2 + h\|\phi^\star\|^2 + \|\phi_h'\|_2^2, \tag{23}$$

in which $\overline{\phi}$ and $\phi^\star$ can be represented on the grid, whereas ϕ_h' cannot. See also Fig. 3.

SMALL SUPERGRID SCALES

In this section, the equations describing $\phi^\star$ are derived. To this end, the small, supergrid density $\phi_i^\star = \frac{1}{2}(\widetilde{\phi}_{i-1/2} - \widetilde{\phi}_{i+1/2})$ is expressed in matrix-vector form as $\phi^\star = S\widetilde{\phi}$. The time rate of change of $\phi^\star$ is obtained by applying the difference operator S to Eq. (11):

$$h\,\partial_t \phi^\star = \nabla_S(\Phi + \tau), \tag{24}$$

where the symmetric $N \times N$ matrix ∇_S is defined by

$$\nabla_S = \tfrac{1}{2}\begin{pmatrix} -2 & 1 & & & 1 \\ 1 & -2 & 1 & & \\ & & & & \\ & & 1 & -2 & 1 \\ 1 & & & 1 & -2 \end{pmatrix}$$

This matrix is negative-semidefinite (like a second derivative). However, it takes on the nature of a gradient if we do not consider it as a linear map of $\widetilde{\phi}$ but as one of $\phi^\star$: $(\nabla_S\widetilde{\phi})_{i-1/2} = -\phi_i^\star + \phi_{i-1}^\star$.

The flux Φ in Eq. (24) can be divided into a convective and a diffusive part. So, we get

$$h\,\partial_t \phi^\star = \nabla_S\left(c(\overline{u},\overline{\phi}) - \tfrac{2\nu}{h}\,\phi^\star + \tau\right) \tag{25}$$

where the convective contribution is described by means of the vector c with components $c_i = \overline{u}_i\overline{\phi}_i$ with $i = 1,\cdots,N$. The convective term in Eq. (25) depends only on the density $\overline{\phi}$ and the velocity $\overline{u}$ of the large eddies. To see what happens if no model is used, we take $\tau = 0$ in Eq. (25). The residual density $\phi^\star$ is then driven by the large eddies, that is the large eddies produce $\phi^\star$ and that's the only way they can be produced. *Thus $\phi^\star$ is subordinate to $\overline{\phi}$.* But if the large eddies increase the amount of residual density, then the dynamics are not closed; in a closed system large eddies should only transport and dissipate themselves. Effectively the dissipation of the large eddies falls short if they produce $\phi^\star$. In conclusion, if $\phi^\star$ is produced by the large eddies then τ should not be zero.

MODELING SCALE SEPARATION

Eq. (23) implies that the dissipation of energy breaks down into three parts:

$$\mathrm{d}_t\,\|\phi\|_2^2 = h\,\mathrm{d}_t\,\|\overline{\phi}\|^2 + h\,\mathrm{d}_t\,\|\phi^\star\|^2 + \mathrm{d}_t\,\|\phi_h'\|_2^2. \tag{26}$$

The last part, the subgrid dissipation, vanishes according to Eq. (19); hence the above right-hand side consists exclusively of supergrid contributions. Suppose the system for the large eddies is not well closed. Then the large eddies may generate smaller scales, so $\mathrm{d}_t\,\|\phi^\star\|^2 > 0$. Eq. (26) then implies $\mathrm{d}_t\,\|\phi\|_2^2 > h\,\mathrm{d}_t\,\|\overline{\phi}\|^2$, meaning the large eddies dissipate less energy than the full system. In that case the dissipation model is insufficient, and we enforce

$$\mathrm{d}_t\,\|\phi^\star\|^2 = 0. \tag{27}$$

so that

$$\mathrm{d}_t\,\|\phi\|_2^2 = h\,\mathrm{d}_t\,\|\overline{\phi}\|^2.$$

This ensures the correct total dissipation, though only in a global sense. In the absense of a model τ, it may also occur that $\mathrm{d}_t\,\|\phi^\star\|^2 < 0$, either because Eq. (25) is dominated by viscous dissipation (that is, the dynamics is resolved) or because energy transfers from residual to large scales (backscatter). Since $\phi^\star$ is subordinate to $\overline{\phi}$, backscatter must originate from τ. Since backscatter is difficult to model we simply set $\tau = 0$ if $\mathrm{d}_t\,\|\phi^\star\|^2 < 0$. Combined with Eq. (27), this yields

$$\mathrm{d}_t\,||\phi^\star||^2 \leq 0, \tag{28}$$

for any time t, i.e., *no residual density is produced*. Note that our reasoning implicitly relies on the 2-norm, though alternative norms could be considered. Interestingly, taking the 1-norm in Eq. (28) results into total variation diminishing (TVD) schemes.

Inequality (28) can be rewritten using Eq. (24). Thus we get

$$\nabla_S\phi^\star\cdot(\Phi+\tau)\le 0, \tag{29}$$

Note that we are considering periodic boundary conditions. As only a requirement is imposed on the component of τ in the direction of the vector $\nabla_S\phi^\star$, we take

$$\tau=-\alpha\nabla_S\phi^\star, \tag{30}$$

where the coefficient $\alpha\ge 0$ is taken *as minimally as possible*. This leads to

$$\alpha=\frac{(\nabla_S\phi^\star\cdot\Phi)_+}{\|\nabla_S\phi^\star\|^2}, \tag{31}$$

where the positive part in the denominator is given by $(\nabla_S\phi^\star\cdot\Phi)_+=\frac{1}{2}(\nabla_S\phi^\star\cdot\Phi+|\nabla_S\phi^\star\cdot\Phi|)$. Note that taking the positive part implies that Eq. (27) is satisfied in the case of forward scatter and Eq. (28) holds in the case of backward scatter.

IMPROVING THE CONSISTENCY

We recall that the exact flux at x_i is given by

$$F_i=\overline{u}_i\overline{\phi}_i-\nu\frac{\widetilde{\phi}_{i+1/2}-\widetilde{\phi}_{i-1/2}}{h}+\tau(x_i;\delta). \tag{32}$$

To approximate the leading-order term of τ, we write down a similar expression with δ replaced by 2δ:

$$F_i={}^2\overline{u}_i\,{}^2\overline{\phi}_i-\nu\frac{\overline{\phi}_{i+1}-\overline{\phi}_{i-1}}{\delta}+\tau(x_i;2\delta). \tag{33}$$

Here, the densities in the convective part are integrated over 2δ. The corresponding box filter is given by

$${}^2\overline{\phi}_i=\frac{1}{2\delta}\int_{x_i-\delta}^{x_i+\delta}\phi(x,t)\,dx=\tfrac{1}{2}\,(\overline{\phi}_{i-1}+\overline{\phi}_{i+1}).$$

Subtracting Eq. (32) from Eq. (33) gives an expression for the difference $\tau(x_i;2\delta)-\tau(x_i;\delta)$. This difference is approximately equal to 3 times the leading-order term assuming that τ is dominated by its $\mathcal{O}(\delta^2)$ term. Accordingly, we can obtain an $\mathcal{O}(\delta^4)$ approximation τ_0 of τ which yields a welcome improvement of the large-scale components of the flux, but does not provide a good description of the dissipation that takes place on the smallest scales. Therefore, we take

$$\tau=\tau_0-\alpha\nabla_S\phi^\star, \tag{34}$$

instead of Eq. (30), where the coefficient $\alpha\ge 0$ is determined such that $(\Phi+\tau_0-\alpha\nabla_S\phi^\star)\cdot\nabla_S\phi^\star\le 0$ and α is again taken as minimally as possible:

$$\alpha=\frac{(\nabla_S\phi^\star\cdot(\Phi+\tau_0))_+}{\|\nabla_S\phi^\star\|^2}. \tag{35}$$

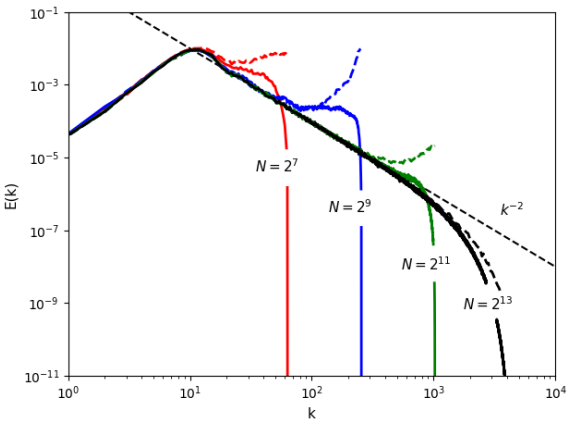

Figure 4. Energy spectra obtained without using any model.

FIRST RESULTS

This section covers first results of numerical simulations. It is intended as an elementary evaluation of the concept; hence the focus is on demonstrating the viability of the idea outlined in this paper in its early stages of development. To this end, we consider Burger's equation, that is we take $u=\frac{1}{2}\phi$ and $\nu=5\,10^{-4}$. As in Maulik & San (2018), we consider a decaying turbulence problem on the domain $[0,2\pi]$ with periodic boundary conditions. The initial energy spectrum is given by $E(k)=Ak^4\exp(-(k/k_0)^2)$, where the constant A is taken such that $\int_0^\infty E(k)dk=\frac{1}{2}$. This leads to $A=2k_0^{-5}/(3\sqrt{\pi})$. The wave number k_0 at which the initial energy spectrum peaks is set to $k_0=10$. Thus the magnitudes of the initial density in Fourier space are $|\hat{\phi}_k|=\sqrt{2E(k)}$. The initial density is obtained by incorporating a random phase $\hat{\phi}_{k,m}(0)=\sqrt{2E(k)}\exp(\mathrm{i}2\pi R_m(k))$, where $R_m(k)$ denotes a random number (uniformly distributed) between 0 and 1 at wave number k. In total $M=512$ initial conditions with randomly sampled phases are computed. Each of them is integrated in time until $t=0.1$ using the forward Euler method. The energy content has decreased by a factor of 10 at $t=0.1$; the maximum dissipation rate occurs at about $t=0.05$. At the end of each simulation the box-filtered density $\overline{\phi}$ is determined from the grid-filtered density $\widetilde{\phi}$. Finally, ensemble averaged energy spectra at $t=0.1$,

$$\frac{1}{M}\sum_{m=1}^{M}\tfrac{1}{2}|\hat{\overline{\phi}}_{k,m}(0.1)|^2 \tag{36}$$

are computed for qualitative assessments of the results of the numerical simulations. For comparison a reference energy spectra has been determined with the help of direct numerical simulation (DNS). Fig. 4 shows energy spectra obtained without using any model. These results are computed from Eqs. (11)-(13) in which $\tau_i=0$ for $i=1,\ldots,N$. The number of gridpoints N varies between 2^7 and 2^{13}. The grid with the smallest width resolves (almost) all physically relevant length scales. The corresponding spectrum displays the k^{-2} scaling characteristic of 1D Burgers turbulence. The underresolved simulations exhibit the typical pile-up of energy near the end of their spectrum; hence these coarse-grid simulations obviously lack a model that extracts energy from the smallest resolved scales. Since no model is applied here, unfiltered, raw data from the finite volume simulation can also be considered. Therefore, the dashed graphs in Fig. 4 show (36) with $\overline{\phi}$ replaced by $\widetilde{\phi}$. The difference between the dashed and solid

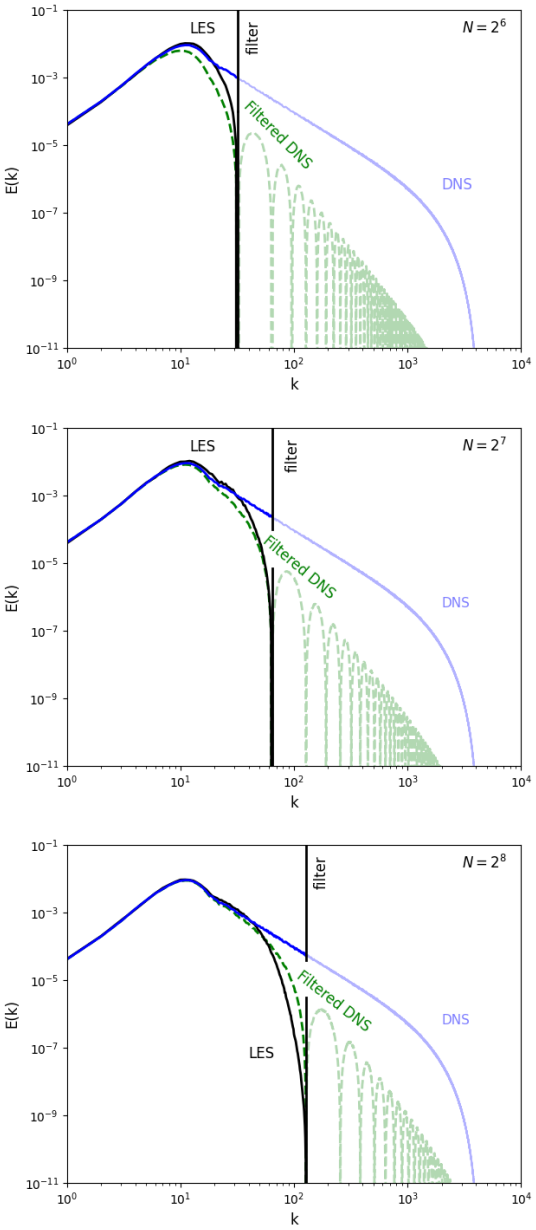

Figure 5. Energy spectra obtained with LES model (34)-(35). The filtered DNS data is represented by the dashed graph; the solid graphs correspond to LES and DNS.

graphs in Fig. 4 corresponds to $\|\widetilde{\phi}\|^2 - \|\overline{\phi}\|^2 = \|\phi^\star\|^2$. The $N = 2^{13}$ DNS provides the reference spectrum for the large eddy simulations. They use $N = 2^q$ gridpoints, where q varies from 6 to 10. The number of timesteps is 2^{q-3}, which results in a maximum CFL number of approximately 0.3. Simulations at lower resolutions ($N = 2^5$, e.g.) give inaccurate results because the peak of the initial energy spectrum is not represented well. In other words, $N = 2^6$ is about the lower limit for which the initial spectrum is represented to a moderate extend. Fig. 5 shows that the energy calculated with the model given by Eqs. (34)-(35) does not pile up; it decreases monotonically at the end of the spectrum. The LES spectrum matches that of the DNS well for large scales of motion and follows the filtered DNS spectrum near the LES cutoff. The DNS data is here filtered using the box filter (1) with filter length $\delta = 2h$. Note that its convolution kernel of the box filter (1) leads to the oscillatory behavior of the filtered DNS spectrum. The first zero of the convolution kernel is $k\delta = 2\pi$. Hence, the LES spectrum consists of all wave numbers k smaller than $2\pi/\delta$. The largest LES wave number $k\delta = 2\pi$ is indicated by "filter" in Fig. 5.

For $N \geq 2^9$, the wave number at which the differences become visible hardly depends on the comparison we make: the wave number at which the LES spectrum starts to deviate from that of the filtered DNS is also approximately the wave number at which the LES spectrum starts to deviate from the (unfiltered) DNS spectrum. From Fig. 5 it can be seen that the graphs of the LES spectrum coincide with the characteristic k^{-2} Burgers' spectrum for a range of wavenumbers. Apart from the $N = 2^6$ grid. This grid is too coarse to capture the first part of the inertial range. Nevertheless, the energy spectrum (around the peak) is approximated well. In conclusion, the scale separation model (34)-(35) can be used to simulate decaying Burgers' turbulence. In itself this is a fairly good result. However, we cannot draw any conclusions about the suitability for LES of 3D turbulence. Further research is needed for that.

REFERENCES

Agdestein, S.D. & Sanderse, B. 2025 Discretize first, filter next: learning divergence-consistent closure models for large-eddy simulation. *Journal of Computational Physics* **522**, 113577.

Geurts, B.J. 2009 Analysis of errors occurring in large eddy simulation. *Philosophical Transactions: Mathematical, Physical and Engineering Sciences* **367**, 2873–2883.

Maulik, R. & San, O. 2018 Explicit and implicit les closures for burgers turbulence. *Journal of Computational and Applied Mathematics* **327**, 12–40.

Pope, S.B. 2004 Ten questions concerning large-eddy simulation of turbulent flows. *New Journal of Physics* **6**, 1–124.